Inorganic Chemistry

pubs.acs.org/IC

Article

Photoconducting Devices with Response in the Visible−Near-Infrared Region Based on Neutral Ni Complexes of Aryl-1,2-dithiolene Ligands

Anna Pintus,* Lucia Ambrosio, M. Carla Aragoni, Maddalena Binda, Simon J. Coles, Michael B. Hursthouse, Francesco Isaia, Vito Lippolis, Giammarco Meloni, Dario Natali, James B. Orton, Enrico Podda, Marco Sampietro, and Massimiliano Arca*

Cite This: https://dx.doi.org/10.1021/acs.inorgchem.0c00491

Read Online

ACCESS | Metrics & More | Article Recommendations | Supporting Information

ABSTRACT: Metal bis(1,2-dithiolene) complexes belonging to the class $[Ni(Ar\text{-}edt)_2]^{x-}$ [Ar-edt^{2-} = arylethylene-1,2-dithiolate; Ar = phenyl, ($\mathbf{1}^{x-}$), 2-naphthyl ($\mathbf{2}^{x-}$); x = 0 and 1] were fully characterized by NMR, UV−visible−near-infrared (UV−vis−NIR), diffuse reflectance, and FT-IR spectroscopy, as well as cyclic voltammetry and single-crystal X-ray diffraction analysis. These complexes have emerged as new photoconducting materials that allowed for the development of a prototype of photodetectors with response in the vis−NIR region. The photodetecting devices showed in some cases quantum efficiencies orders of magnitude higher than those of previously reported 1,2-dithiolene systems.

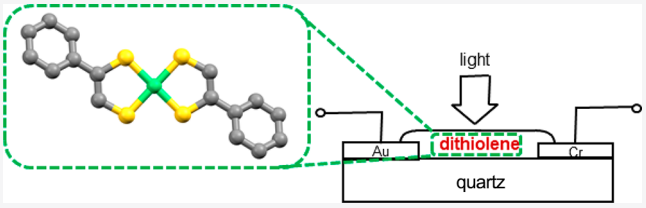

INTRODUCTION

Because of the unique combination of optical, conductive, magnetic, and catalytic properties, transition metal 1,2-dithiolene complexes have attracted ever-increasing attention from the scientific community since the earliest reports in the 1960s.[1−5] While molybdenum and tungsten 1,2-dithiolene complexes have shown enzymatic activity,[6,7] bis(1,2-dithiolene) compounds featuring d^8 metal ions have been employed as materials in disparate fields, ranging from optics[4c,8] to laser Q-switching and mode-locking,[9−11] superconductors,[12,13] water photosplitting,[14] and olefin purification.[15] All of the aforementioned applications depend on the electronic structure of this class of compounds,[5b] which gives rise to crucial properties such as a high degree of π-delocalization, molecular planarity,[3f] widely tunable and reversible redox behavior,[3e,16−19] intense electrochromic visible−near-infrared (vis−NIR) absorption,[3g,20] and high thermal and photochemical stabilities.[21] In particular, the "non-innocent" character of 1,2-dithiolene ligands has been shown to play a pivotal role in the chemistry of their transition metal complexes.[22] In recent years, bis(1,2-dithiolene) compounds featuring d^8 metal ions have also been investigated as new potential materials in a wide-span range of optoelectronic devices,[23] such as n-channel and ambipolar channel field effect transistors (FETs),[24−29] heterojunction photovoltaic devices,[30] second- or third-order nonlinear optical (NLO) devices,[11,31−34] and NIR liquid-crystal devices.[35] The photoconducting properties of metal bis(1,2-dithiolene) complexes have also been investigated by a number of research groups.[36] For instance, Naito and co-workers reported on the giant photoconductivity shown by the NMQ[Ni(dmit)$_2$] molecular salt in the UV region (NMQ = *N*-methylquinolinium, dmit^{2-} = 1,3-dithiol-2-thione-4,5-dithiolate),[37] while the photodetection properties of bis(4-dimethylaminodithiobenzil)nickel(II) were investigated using a Schottky type device.[38]

In this context, some of the authors reported on the photoconductive properties of several group 10 metal bis(1,2-dithiolene) complexes for the development of devices of importance in telecommunications, such as photodetectors and photoswitches, operative in all three optical fiber windows.[39−43] In particular, several neutral complexes belonging to the classes [M(R,R′-timdt)$_2$] and [Ni(Et-dmet)$_2$] (R,R′-timdt^{2-} = *N*,*N*′-disubstituted 2-thioxoimidazoline-4,5-dithiolate, R = Et, R′ = Et and pentyl, M = Ni, Pd, and Pt;[39,40] Et-dmet^{2-} = *N*-ethyl-2-thioxothiazoline-4,5-dithiolate)[41] were reported to display tunable, wavelength-selective photoconductivity centered on their NIR absorption (λ_{max} ∼ 1000 nm) in a wavelength region between the second (850−1000 nm) and third (1500−1800 nm) windows of optical fibers.[41] Monoreduced radical anions $[Pt(R,R'\text{-}timdt)_2]^-$ (R = Et; R′ = Et, pentyl),[42,43] whose NIR absorption falls at longer

Received: February 18, 2020

wavelengths ($\lambda_{max} \sim 1400$ nm for M = Ni and Pt; 1700 nm for M = Pd) exhibited solid-state photoconducting properties in the third optical fiber window.

The synthesis and characterization of variously functionalized aryl-1,2-dithiolene ligands (Ar-edt^{2-}) and the neutral and monoanionic relevant nickel complexes [Ar = phenyl (Ph),[44] *p*-trifluoromethyl,[24] *p*-nitro, *p*-fluoro, *p*-chloro, and *p*-bromo-phenyl][45] were reported during the past decades. The reactivity of some members of this class of metal complexes was also explored.[44,46] Naphthalene- and coumarin-substituted dithiolene ligands were exploited as selective markers of the Ni^{2+} ion.[47]

Following our previous studies on d^8 metal complexes bearing Ar-edt^{2-} ligands showing potential-controlled spectroscopic and second-order NLO properties,[48,49] and pursuing our interest in photoconducting bis(1,2-dithiolene) complexes, we describe here the synthesis, characterization, and the development of a novel photodetector with response in the visible−NIR region based on the class $[Ni(Ar\text{-}edt)_2]^{x-}$ of complexes [Ar = Ph, ($\mathbf{1}^{x-}$), 2-naphthyl ($\mathbf{2}^{x-}$); x = 0, 1, and 2; Scheme 1].

Scheme 1. Synthesis of Compounds $(TBA^+)(\mathbf{1}^-\text{−}\mathbf{2}^-)$ and Neutral Complexes 1−2[a]

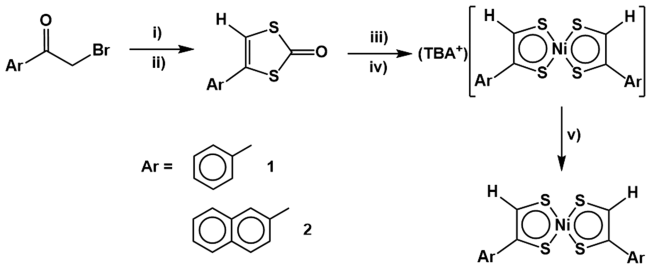

[a]The aryl substituents are depicted in the *cis* conformation: (i) *i*PrOCS$_2$K in acetone; (ii) $HClO_4$ concd.; (iii) EtOK in EtOH; (iv) $NiCl_2 \cdot 6H_2O$, $(TBA^+)(I^-)$; (v) I_2 in CH_3CN.

EXPERIMENTAL SECTION

Materials and Methods. Solvents (reagent-grade) were purchased from Honeywell, VWR, and Merck. Reaction solvents were dried by using standard techniques when required. $CDCl_3$ was stored on activated 4 Å molecular sieves before use. Reagents were purchased from Honeywell, Alfa Aesar, and Sigma-Aldrich and used without further purification. When required, manipulations were performed using standard Schlenk techniques under dry nitrogen atmosphere. Melting points were recorded on a FALC melting point apparatus mod. C (up to 300 °C) and are uncorrected. Elemental analyses were performed with a CHNS/O PE 2400 series II CHNS/O elemental analyzer (T = 925 °C). FT-IR spectra were recorded with a Thermo-Nicolet 5700 spectrometer at room temperature. KBr pellets with a KBr beam splitter and KBr windows (4000−400 cm^{-1}, resolution 4 cm^{-1}) were used. ^{1}H NMR measurements were carried out in $CDCl_3$ at 25 °C, using a Bruker Advance 300 MHz (7.05 T) spectrometer at the operating frequency of 300.13 MHz. Chemical shifts are reported in ppm (δ) and are calibrated to the solvent residue. Cyclic voltammetry (CV) and differential pulsed voltammetry (DPV) measurements were recorded at 25 °C in anhydrous CH_2Cl_2 at scan rate 0.1 V s^{-1}, using a Metrohm Autolab PGSTAT 10 potentiostat at 20 °C in a Metrohm voltammetric cell, with a combined working and counter Pt electrode and a standard Ag/AgCl (in KCl 3.5 M) reference electrode. All potentials are referred to the Fc^+/Fc couple, used as an internal standard. Tetrabutylammonium hexafluorophosphate was used as a supporting electrolyte (C = 1 × 10^{-2} M). Absorption spectra were recorded at 25 °C in CH_2Cl_2 in a quartz cell of 10.00 mm optical path with a Thermo Evolution 300 (190−1100 nm) spectrophotometer. Spectrophotometric titrations of $(TBA^+)(\mathbf{1}^-)$ and $(TBA^+)(\mathbf{2}^-)$ (TBA = tetrabutylammonium; C = 3.0 × 10^{-5} M; V = 3.00 mL) with molecular diiodine (C = 3.0 × 10^{-3} M) were carried out in CH_2Cl_2 up to the molar range of diiodine/dithiolene 2.5:1. Diiodine solutions were previously titrated by suspending the solution (1 mL) in distilled water (50 mL), adding excess KI and titrating with a standard solution of sodium thiosulfate (0.010 M) with a Metrohm 776 Dosimat automatic buret. Diffuse reflectance measurements were carried out on an Agilent Cary 5000 UV−vis−NIR dual-beam spectrophotometer equipped with a diffuse reflectance accessory. Spectra were corrected for the change in the detector (PMT and InGaAs) at 800 nm.

X-ray Diffraction Measurements. X-ray single-crystal diffraction data for 4-phenyl-[1,3]dithiol-2-one (Table S1) were collected upon Bruker-Nonius Mo Kα FR591 diffractometer, equipped with Bruker-Nonius Roper CCD camera, kappa-goniostat goniometer, and a low-temperature device [operating at T = 120(2) K]. The data were indexed and processed using DENZO[50] and COLLECT.[51] The structure was solved by SHELXS-97[52] and refined using SHELXL-97[53] with least squares minimization. X-ray single-crystal diffraction data for **1** and **2** (Table S1) were collected upon Rigaku FRE+ Mo Kα diffractometer, equipped with HF Varimax confocal mirrors, an AFC12 goniometer, a HG Saturn 724+ detector, and an Oxford Cryosystems low-temperature device (operating at T = 100(2) K). The data were indexed and processed using Crystal Clear-SM Expert 3.1 b22.[54] The structure was solved by Superflip and refined with SHELXL-97,[53] using least squares minimization within the WinGX suite of software.[55] X-ray single-crystal diffraction data for $(TBA^+)(\mathbf{1}^-)$ (Table S1) were collected upon a Rigaku FRE+ diffractometer, equipped with HF Varimax confocal mirrors, an AFC12 goniometer, a HG Saturn 724+ detector, and an Oxford Cryosystems low-temperature device (operating at T = 100(2) K). The data were indexed and processed using CrysAlisPro.[56] The structure was solved with the SHELXT structure solution program[57] with the Intrinsic Phasing solution method and by using Olex2[58] as the graphical interface. The model was refined with version 2018/3 of ShelXL[59] using least squares minimization. X-ray single-crystal diffraction data for $(TBA^+)(\mathbf{2}^-)$ (Table S1) were collected at 120(2) K upon Daresbury SRS station 9.8, upon a Bruker SMART diffractometer, equipped with silicon 111 monochromator, and an APEX CCD detector, and a low-temperature device (operating at T = 120(2) K). The data were indexed and processed using Bruker SAINT[60] and SADABS.[61] The structure solved by SHELXS-97[52] and refined on using SHELXL-97[53] with least squares minimization. CCDC 1953278 (4-phenyl-[1,3]dithiol-2-one), CCDC 1953277 [$(TBA^+)(\mathbf{1}^-)$], CCDC 1009772 [$(TBA^+)(\mathbf{2}^-)$], CCDC 1953275 (**1**), and CCDC 1953276 (**2**) contain the supplementary crystallographic data for this paper. These data can be obtained free of charge from The Cambridge Crystallographic Data Centre.

Photophysical Measurements. Photoconductivity measurements were performed by using prototype lateral devices prepared by casting a $CHCl_3$ solution ($C \approx 1$ mg mL^{-1}) of each active complex on a quartz substrate with previously lithographed gold/chromium electrodes with interelectrode spacings L = 6 μm. The devices were kept in vacuum ($P < 10^{-3}$ mbar) and irradiated with a set of light-emitting diodes (LEDs) emitting a power density of a few mW cm^{-2} (calibration was obtained by means of a silicon photodetector). Photodetecting properties were investigated by applying an external bias voltage V_{BIAS}= 60 V and measuring the direct current (dc) photocurrent by means of a semiconductor parameter analyzer (Agilent B1500A). In order to calculate the external quantum efficiency (EQE) we computed the ratio between the photocurrent divided by the unit charge q and the number of photons impinging on the device area per second.

Synthesis. Phenyl- and 2-naphthyl-[1,3]dithiol-2-one were synthesized according to previously published procedures.[48]

Synthesis of $(TBA^+)(\mathbf{1}^-)$. An ethanol solution of KOH (45 mL; 0.25 g; 4.03 mmol) was added dropwise to 4-phenyl-[1,3]dithiol-2-one

https://dx.doi.org/10.1021/acs.inorgchem.0c00491
Inorg. Chem. XXXX, XXX, XXX−XXX

(30 mL of EtOH; 0.21 g; 1.09 mmol) under a dinitrogen inert atmosphere. After addition of solutions of $NiCl_2·6H_2O$ (15 mL; 0.13 g; 0.55 mmol) and $(TBA^+)(I^-)$ (15 mL; 0.21 g; 0.57 mmol) in ethanol, the volume of the reaction mixture was reduced under reduced pressure, and the precipitate was collected by filtration. Crystals suitable for X-ray diffraction were obtained by slow infusion of diethyl ether into a dichloromethane solution of the complex. Yield 0.240 g (70.6%). Mp 146−147 °C. FT-IR: $\tilde{\nu}$ = 3025 (w), 2958 (s), 2941 (m), 2871 (m), 1589 (s), 1571 (w), 1493 (m), 1479 (m), 1454 (s), 1430 (s), 1375 (m), 1360 (w), 1220 (w), 1208 (s), 1180 (w), 1152 (w), 1104 (w), 1071 (w), 1029 (w), 932 (m), 904 (w), 879 (w), 836 (m), 751 (vs), 691 (s), 679 (w), 615 cm^{-1}(w). UV−vis−NIR (CH_2Cl_2): λ (ε) = 261 (40 500), 320 (35 800), 531 (220), 942 nm (11 600 M^{-1} cm^{-1}). Elemental analysis calcd (%) for $C_{32}H_{48}NNiS_4$: C 60.65, H 7.63, N 2.21. Found: C 59.01, H 7.46, N 2.15.

Synthesis of $(TBA^+)(\mathbf{2}^-)$. $(TBA^+)(\mathbf{2}^-)$ was synthesized as described for $(TBA^+)(\mathbf{1}^-)$ starting from 4-(2-naphtyl)-[1,3]dithiol-2-one. Crystals suitable for X-ray diffraction were obtained by slowly cooling down to room temperature a previously heated (130 °C) solution of the product in diethyl ether/dichloromethane (30/2 mL) in a high-pressure Aldrich tube. Yield 0.170 g (51.2%). Mp 185−186 °C. FT-IR: $\tilde{\nu}$ = 3053 (w), 3013 (w), 2959 (s), 2938 (m), 2931 (m), 2870 (m), 1621 (m), 1592 (m), 1571 (vw), 1482 (s), 1445 (vs), 1425 (w), 1381 (s), 1341 (m), 1271 (vw), 1254 (w), 1229 (s), 1205 (w), 1172 (m), 1145 (w), 1124 (vw), 1107 (vw), 1069 (vw), 1019 (vw), 967 (m), 924 (vw), 893 (m), 881 (s), 864 (m), 816 (s), 795 (vs), 781 (s), 767 (m), 781 (s), 751 (s), 736 (vw), 645 (m), 625 (w), 647 (vw), 474 (s), 415 cm^{-1}(vw). UV−vis−NIR (CH_2Cl_2): λ (ε) = 260 (47 400), 320 (41 900), 532 (2600), 946 nm (13 500 M^{-1} cm^{-1}). Elemental analysis calcd (%) for $C_{40}H_{52}NNiS_4$: C 65.47, H 7.14, N 1.91. Found: C 65.32, H 6.34, N 1.85.

Synthesis of **1**. An anhydrous acetonitrile solution of I_2 (20 mL; 0.090 g; 3.4 mmol) was added dropwise to a solution of $(TBA^+)(\mathbf{1}^-)$ in the same solvent (75 mL of CH_3CN; 0.22 g; 3.2 mmol) under a dinitrogen inert atmosphere. The resulting precipitate was collected by filtration. Crystals suitable for X-ray diffraction were obtained by slow infusion of diethyl ether into a dichloromethane solution of the complex. Yield 0.120 g (97.5%). Mp 171−172 °C. FT-IR: $\tilde{\nu}$ = 3017 (vw), 1446 (w), 1381 (s), 1367 (vs), 1331 (w), 1227 (w), 1192 (s), 1132 (vw), 1031 (vw), 958 (w), 859 (s), 840 (m), 807 (w), 754 (s), 690 (s), 613 (vw), 475 cm^{-1}(vw). UV−vis−NIR (CH_2Cl_2): λ (ε) = 253 (22 500), 270 (23 000), 303 (42 000), 577 (1500), 816 nm (22 900 M^{-1} cm^{-1}). Elemental analysis calcd (%) for $C_{16}H_{12}NiS_4$: C 49.12, H 3.09. Found: C 48.76, H 3.02. ^1H NMR (300 MHz, $CDCl_3$): δ = 9.72 (s, 2H), 8.00 (d, 4H), 7.52−7.44 (m, 6H) ppm.

Synthesis of **2**. Compound **2** was synthesized following the procedure described for **1**, starting from $(TBA^+)(\mathbf{2}^-)$. Crystals suitable for X-ray diffraction were obtained by slow infusion of diethyl ether into a chloroform solution of the complex. Yield 0.070 g (90%). Mp 232−233 °C. FT-IR: $\tilde{\nu}$ = 3051 (vw), 3021 (vw), 1467 (w), 1390 (vs), 1383 (vs), 1345 (vs), 1280 (w), 1252 (vs), 1200 (m), 1173 (vs), 1158 (s), 935 (m), 899 (s), 882 (m), 849 (m), 809 (vw), 786 (s), 770 (w), 737 (m), 676 (vw), 461 cm^{-1}(m). UV−vis−NIR (CH_2Cl_2): λ (ε) = 250 (45 100), 308 (51 100), 576 (1840), 861 nm (27 500 M^{-1} cm^{-1}). Elemental analysis calcd (%) for $C_{24}H_{16}NiS_4$: C 58.67, H 3.28. Found: C 58.21, H 2.82. ^1H NMR (300 MHz, $CDCl_3$): δ = 9.90 (s, 2H), 8.10 (d, 4H), 8.01−7.96 (m, 4H), 7.60−7.55 (m, 6H) ppm.

Theoretical Calculations. Theoretical calculations were performed on $\mathbf{1}^{x-}$ and $\mathbf{2}^{x-}$ (x = 0 and 1) at the density functional theory (DFT)[62] level with the Gaussian 16 (rev. B.01)[63] suite of programs on a IBM x3755 server with four 12-core processors and 64 Gb of RAM (OS: SUSE Linux Enterprise Server 11 SP3). The mPW1PW functional[64] was adopted, in combination with the full-electron split-valence basis sets (BSs) including polarization functions (def2-SVP)[65,66] for light atomic species (C, H, S) and the LanL08(d) BS[67] with effective core potentials[68] for nickel. Basis sets were obtained from Basis Set Exchange and Basis Set EMSL Library.[69] A series of preliminary calculations were performed by using **1** in its *cis* conformation as a model compound. The complex was thus optimized both in the closed-shell restricted electron configuration and in the broken-symmetry configuration of the diradical form $[Ni^{II}(L^{\bullet-})_2]$. The diradical character n_{rad} was calculated from the total spin operator S^2 according to eq 1[70] and was found to be as large as 20.41%.

$$n_{rad} = 200 \sin^2 \vartheta = 100(1 - \sqrt{1 - S^2}) \quad (1)$$

The geometries of neutral complexes **1** and **2** were optimized in the predominant closed-shell restricted configuration. Geometry optimizations were performed on the *cis* and *trans* isomers starting from structural data, when available, and were regularized by letting the model complexes belong to an ideal C_2 point group (Tables S3−S10). Calculations were carried out also in CH_2Cl_2, implicitly taken into account by means of the Polarizable Continuum Model in its Integral Equation Formalism variant (IEF-PCM) describing the cavity of the complexes within the reaction field (SCRF) through a set of overlapping spheres (Tables S11 and S12).[71] Tight SCF convergence criteria (*SCF* = *tight* keyword) and fine numerical integration grids (*Integral* = *ultrafine* keyword) were used, and the nature of the minima of each optimized structure was verified by harmonic frequency calculations (*freq* = *Raman* keyword). PES scans were performed on $\mathbf{1}^{x-}$ and $\mathbf{2}^{x-}$ (x = 0 and 1; *cis* and *trans* isomers) by imposing the rotation of the aromatic rings (between 0 and 180°, steps of 10°) and optimizing the resulting geometry at each rotational step (*opt* = *modredundant* keyword). A natural population analysis was carried out at the optimized geometries using the natural bonding orbital (NBO) partitioning scheme (Table S13).[72] Electronic transition energies and oscillator strength values were calculated at TD-DFT level (100 states; Table S14). The programs GaussView 6.0.16,[73] Molden 5.9,[74] and Chemissian 4.53[75] were used to investigate the optimized structures and the shapes of Kohn−Sham molecular orbitals. The software GaussSum 2.1[76] was used to calculate the contributions of singly excited configurations to each electronic transition.

RESULTS AND DISCUSSION

Synthesis. The synthesis of metal bis(1,2-dithiolene) complexes is commonly hampered by the tendency of 1,2-dithiolates to polymerize or decompose.[2b,77] Accordingly, ethylene-1,2-dithiolates must be protected before being reacted with the desired metal salts. One of the most frequently encountered synthetic procedures consists of reacting α-haloketones with alkylxanthate anions to give the corresponding α-ketoxanthate esters, which give the relevant vinylene dithiocarbonates in strongly acidic media (Scheme 1).[45,78] Following this route, the 4-phenyl- and 4-(2-naphtyl)-[1,3]-dithiol-2-ones were synthesized as previously described[48,49] (see details on the X-ray diffraction analysis of 4-phenyl-[1,3]dithiol-2-one in Table S1 and Figure S1). Complexes $(TBA^+)(\mathbf{1}^-)$ and $(TBA^+)(\mathbf{2}^-)$ were synthesized by treating the corresponding aryl-[1,3]dithiol-2-ones with nickel chloride hexahydrate in the presence of tetrabutylammonium (TBA) iodide. The neutral complexes **1** and **2** were obtained by quantitative oxidation of $(TBA^+)(\mathbf{1}^-)$ and $(TBA^+)(\mathbf{2}^-)$ with molecular diiodine in MeCN solution (Scheme 1).[46,79]

X-ray Diffraction Studies. The crystal structures of $(TBA^+)(\mathbf{1}^-)$ and $(TBA^+)(\mathbf{2}^-)$ (Table S1 and Figures S2 and 1, respectively), the latter being isostructural to the corresponding gold(III) complex,[48] show the central metal ion coordinated in a square-planar fashion, with the ligands assuming *trans* and *cis* conformations, respectively, and the aryl substituents twisted with respect to the dithiolene core by 18.6(2)/18.1(2)° and 26.7(6)/26.9(7)°, respectively. Interestingly, the occurrence of the *cis* conformation found for $(TBA^+)(\mathbf{2}^-)$ (Figure 1) and tetrabutyl ammonium bis(naphthyl-1,2-ethylenedithiolato)gold(III) is uncommon.[48]

https://dx.doi.org/10.1021/acs.inorgchem.0c00491
Inorg. Chem. XXXX, XXX, XXX−XXX

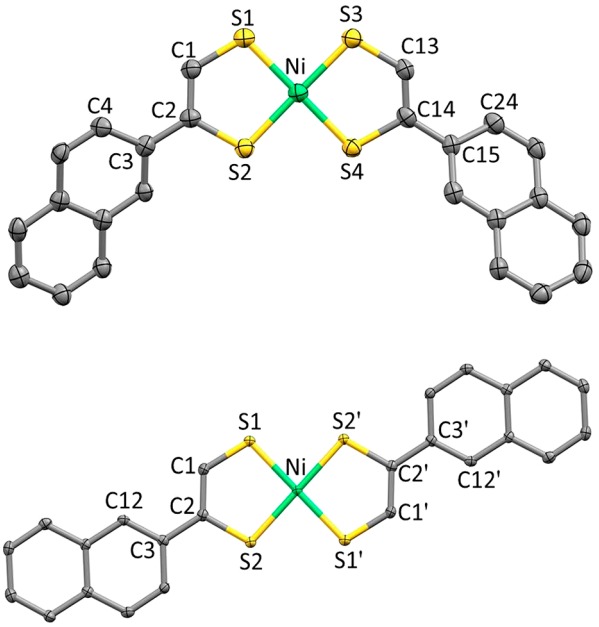

Figure 1. Drawing and atom labeling scheme for the complex anion in $(TBA^+)(\mathbf{2}^-)$ (top) and for **2** (bottom). Thermal ellipsoids are shown at the 60% probability level. Hydrogen atoms were omitted for clarity. Selected bond lengths, angles, and dihedral angles: $\mathbf{2}^-$: Ni−S1 2.147(1), Ni−S2 2.150(1), Ni−S3 2.144(1), Ni−S4 2.148(1), S1−C1 1.717(4), S2−C2 1.732(5), S3−C13 1.706(5), S4−C14 1.747(5), C1−C2 1.361(6), C13−C14 1.349(6) Å; S1−Ni−S2 91.60(5), S3−Ni−S4 91.36(5), S1−Ni−S3 89.11(5), S2−Ni−S4 88.15(4), Ni−S1−C1 103.7(1), Ni−S2−C2 104.8(1), Ni−S3−C13 103.8(1), Ni−S4−C14 105.0(2), S1−C1−C2 121.8(3), S2−C2−C1 118.0(3), S3−C13−C14 123.0(3), S4−C14−C13 116.9(3), C1−C2−C3−C4 26.7(6), C13−C14−C15−C24 26.9(7), C1−S1−Ni−S3 178.4(2), C14−S4−Ni−S2 177.4(2)°. **2**: Ni−S1 2.1229(6), Ni−S2 2.1441(5), S1−C1 1.681(2), S2−C2 1.719(2), C1−C2 1.381(3) Å; S1−Ni−S2 91.5(2), S1−Ni−S2′ 88.45(2), Ni−S1−C1 104.50(8), Ni−S2−C2 104.81(8), S1−C1−C2 121.9(2), S2−C2−C1 117.2(2); C1−C2−C3−C12 2.0(4), C1−S1−Ni−S2′ 179.17 (9)°. ′ = 1 − *x*, −*y*, −*z*.

$(PPh_4^+)(\mathbf{2}^-)$[47] and the other nickel complexes deriving from differently asymmetrically substituted 1,2-dithiolene ligands reported in the literature, namely, $(TBA^+)[Ni(CF_3Ph\text{-}edt)_2]^-$,[24] $(TBA^+)[Ni(FPh\text{-}edt)_2]^-$, $(TBA^+)[Ni(ClPh\text{-}edt)_2]^-$,[45] and all show a *trans* conformation (CF_3Ph = *p*-trifluoromethylphenyl, FPh = *p*-fluorophenyl, ClPh = *p*-chlorophenyl). The conformation does not affect the structural features, and the average Ni−S, C−S, and C−C bond distances found are very similar for $(TBA^+)(\mathbf{1}^-)$ and $(TBA^+)(\mathbf{2}^-)$ (2.144, 1.729, and 1.358 Å and 2.147, 1.725, and 1.355 Å, respectively). These are very similar to those determined for $(PPh_4^+)(\mathbf{2}^-)$ (2.139, 1.721, and 1.358 Å) and $(TBA^+)[Ni(CF_3Ph\text{-}edt)_2]^-$, $(TBA^+)[Ni(FPh\text{-}edt)_2]^-$, and $(TBA^+)[Ni(ClPh\text{-}edt)_2]^-$ (average values 2.141, 1.727, and 1.346 Å, respectively).

In the crystal packing, the complex anions interact to each other and with the TBA^+ countercations by weak S···H contacts [S1···H11A = 2.95, S2···H13B^{i} 2.94, S2···H7^{ii} 3.06 for $(TBA^+)(\mathbf{1})$; S4···H7^{iii} 2.97, S2···H21^{iv} 2.99, S3···H28^{v} 3.04, S2···H27a^{vi} 3.04 Å for $(TBA^+)(\mathbf{2}^-)$; symmetry codes: ^{i} = *x*, 1 + *y*, *z*; ^{ii} = −*x*, *y*, 1/2 − *z*; ^{iii} = 1 − *x*, 1/2 + *y*, 3/2 − *z*; ^{iv} = 1/2 + *x*, 1/2 − *y*, 1 − *z*; ^{v} = 1/2 − *x*, −*y*, 1/2 + *z*; ^{vi} = 1 − *x*, −1/2 + *y*, 1/2 − *z*]. No stacking interactions between complex ions can be observed with Ni···Ni distances no shorter than 10.288 and 8.698 Å for $(TBA^+)(\mathbf{1}^-)$ and $(TBA^+)(\mathbf{2}^-)$, respectively [Figure S3 for $(TBA^+)(\mathbf{2}^-)$]. Single-crystal X-ray diffraction analysis of **1** confirmed the crystallographic data reported previously by Sugimori and co-workers.[44] As expected,[80,81] on passing from the neutral to the corresponding monoanionic species, the C−C and C−S bond lengths are elongated and shortened, respectively [average C−C distances: 1.377 Å for **1**/**2**, 1.356 Å for $\mathbf{1}^-/\mathbf{2}^-$; average C−S distances 1.701 Å for **1**/**2**, 1.714 Å for $\mathbf{1}^-/\mathbf{2}^-$]. Both **1** (Figure S4) and **2** (Figure 1, Table S1) show the complexes in a *trans* conformation, in analogy to the related systems $[Ni(CF_3Ph\text{-}edt)_2]$[24] and $[Ni(ClPh\text{-}edt)_2]$.[45] On the basis of variable-temperature ^{1}H NMR data, it was hypothesized[44] that **1** displays a rapid *cis*/*trans* isomerization in solution, possibly occurring through rotation of the ligand around the metal ion. Accordingly, the room-temperature ^{1}H NMR spectra recorded for **1** and **2** in $CDCl_3$ solution show a single signal for the vinyl proton (H1 in Figure S5) at 9.72 and 9.90 ppm, respectively.

In **1**, the phenyl rings are tilted with respect to the dithiolene ring by 24.42−33.58(10) °; on the contrary, complex molecules in **2** are almost planar, with torsions angles of 2.0(4) ° for the naphthyl substituents. Even in the absence of counterions, no π-stacking interactions are found in the case of the neutral species, with Ni···Ni distances no shorter than 5.010 and 4.639 Å for **1** and **2**, respectively. For both complexes, the packing is mainly governed by edge-to-face interactions involving the aromatic substituents and leading to different herringbone type arrangements (Figures S6 and S7).

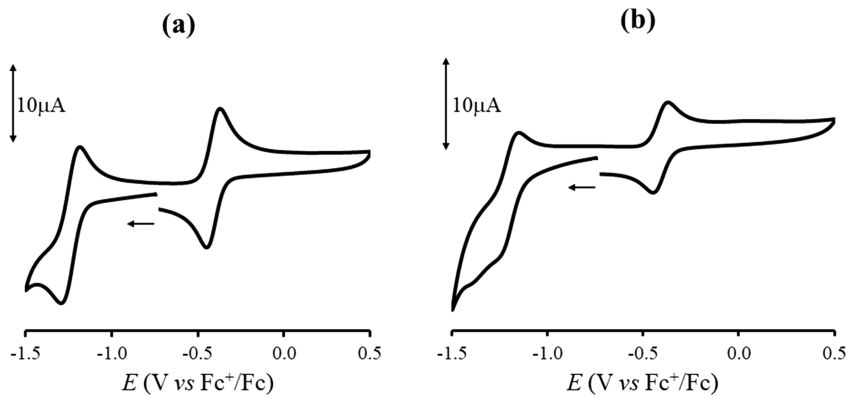

Figure 2. CV data of $(TBA^+)(\mathbf{1}^-)$ (a) and $(TBA^+)(\mathbf{2}^-)$ (b) at a platinum electrode in CH_2Cl_2[25 °C; scan rate 0.100 V s^{-1}; supporting electrolyte $(TBA^+)(PF_6^-)$ 0.1 M].

https://dx.doi.org/10.1021/acs.inorgchem.0c00491
Inorg. Chem. XXXX, XXX, XXX−XXX

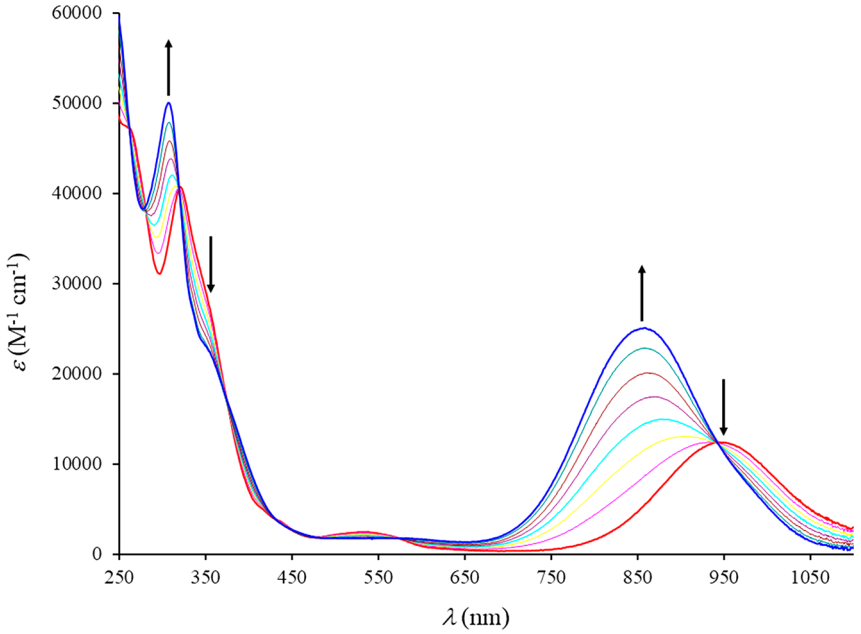

Figure 3. Dilution-corrected UV−vis−NIR spectra recorded during the spectrophotometric titration of a solution of $(TBA^+)(\mathbf{2}^-)$ with I_2 in CH_2Cl_2.

In **1**, symmetry-nonequivalent complex units (Ni1 and Ni2 in Figure S4) pack in staggered sheets through weak S···H and edge-to-face interactions involving alternated C3−C8 and C11−C11 phenyl rings angled of 49.5° [C7−H7···$Cnt_{(C11-C15)}$ 2.87Å, C4−H4···$Cnt_{(C11-C15)}$ 2.73 Å, *a* and *b* in Figure S6]. Similar edge-to-face interactions can be found in complex **2** [C10−H10···$Cnt_{(C3,C4,C5,C6,C11,C12)}$ 2.68 Å, C5−H5···$Cnt_{(C6-C11)}$ 2.64 Å, *a* and *b* in Figure S7]. The herringbone disposition was also engendered in **2** by Ni···$S1^{iii}$ 3.29 Å and S1···$S1^{iv}$ 3.43 Å interactions shown in green and blue in Figure S7.

Electrochemistry and Vis−NIR Spectroscopy. The redox behaviors of $(TBA^+)(\mathbf{1}^-)$ and $(TBA^+)(\mathbf{2}^-)$ were investigated by cyclic voltammetry (CV) in CH_2Cl_2 solution (Figure 2). Two one-electron DPV-tested redox waves were observed for both complexes, falling at about −1.20 and −0.41 V vs the Fc^+/Fc couple (Table S2) and corresponding to the reduction of the complexes to their dianionic forms ($\mathbf{1}^{2-}$ and $\mathbf{2}^{2-}$) and their oxidation to give **1** and **2**. While the oxidation processes involving the $\mathbf{1}^-/\mathbf{1}$ and $\mathbf{2}^-/\mathbf{2}$ couples and the reduction for the $\mathbf{1}^-/\mathbf{1}^{2-}$ couple were found to be reversible ($i_{pc}/i_{pa} \sim 1.0$), reduction for the $\mathbf{2}^-/\mathbf{2}^{2-}$ couple was found to be only quasi-reversible ($i_{pc}/i_{pa} = 0.7$). It should be noted that these findings differ from those previously obtained in acetonitrile for $(TBA^+)(\mathbf{1}^-)$[45] and $(PPh_4^+)(\mathbf{2}^-)$,[47] where an irreversible nature was found for both the reduction and oxidation process.

The oxidation processes leading from $\mathbf{1}^-$ and $\mathbf{2}^-$ to **1** and **2** were investigated by spectrophotometric titration of $(TBA^+)(\mathbf{1}^-)$ and $(TBA^+)(\mathbf{2}^-)$ with diiodine in CH_2Cl_2 solution (Figure 3). Notably the *cis*/*trans* isomerism in solution (see above) does not prevent a spectrophotometric investigation under the hypothesis, confirmed by TD-DFT calculations (see below), that the *cis* and *trans* isomers of each metal complex feature very close UV−vis−NIR absorption spectroscopic features. Accordingly, very well-defined isosbestic points were found during the spectrophotometric I_2 titrations. The UV−vis−NIR electronic absorption spectra of $\mathbf{1}^-$ and $\mathbf{2}^-$ show the characteristic intense NIR absorption bands [λ_{max} = 942 and 946 nm; ε = 11 600 and 13 500 M^{-1} cm^{-1} for $(TBA^+)(\mathbf{1}^-)$ and $(TBA^+)(\mathbf{2}^-)$, respectively], which undergo an hypsochromic shift upon oxidation (λ_{max} = 816 and 838 nm; ε = 26 600 and 27 500 M^{-1} cm^{-1} for **1** and **2**, respectively), as also confirmed by the absorption spectra of **1** and **2** in the same solvent (Figure S8). Solid-state diffuse reflectance spectra recorded for both neutral and monoanionic complexes show an envelope of broad bands resulting in an uninterrupted absorption extending from the UV to the NIR region (Figure S9 for **1** and **2**).

Theoretical Calculations. QM calculations at the density functional theory (DFT)[62] level represent an invaluable tool in understanding the electronic structure of a plethora of compounds, including metal complexes, as they have been extensively exploited to investigate structure/property relationships in a large variety of compounds at an acceptable computational cost. Aimed at elucidating both the redox and optical properties of $\mathbf{1}^{x-}$−$\mathbf{2}^{x-}$, as well as their electronic structure and *cis*/*trans* isomerism, DFT calculations were carried out on the title bis(1,2-dithiolene) Ni neutral and monoanionic complexes. In agreement with previously established approaches on related systems,[48,49,82−86] the mPW1PW hybrid functional[64] was used in combination with full-electron split-valence basis sets, including polarization functions from Schäfer, Horn, and Ahlrichs[65] in the Weigend formulation (def2-SVP)[66] for light atomic species (C, H, S) and the LanL08(d) BS[67] with effective core potentials[68] for nickel.

The redox noninnocence[22,87,88] of 1,2-dithiolene ligands generated a large debate regarding their electronic structure. While paramagnetic monoanionic metal bis(1,2-dithiolene) complexes have been reported as $[M^{III}(\mathbf{L}^{2-})_2]^-$ species[45] or as featuring a dianionic ligand $\mathbf{L}^{2-}$ and monoanionic radical one $\mathbf{L}^{\bullet-}$, i.e., $[M^{II}(\mathbf{L}^{\bullet-})(\mathbf{L}^{2-})]^-$, neutral species have been depicted as closed-shell species (featuring the metal in oxidation states ranging between 0 and IV) or as diradicals formed by a metal dication M^{II} and two radical monoanionic antiferromagneti-

https://dx.doi.org/10.1021/acs.inorgchem.0c00491
Inorg. Chem. XXXX, XXX, XXX−XXX

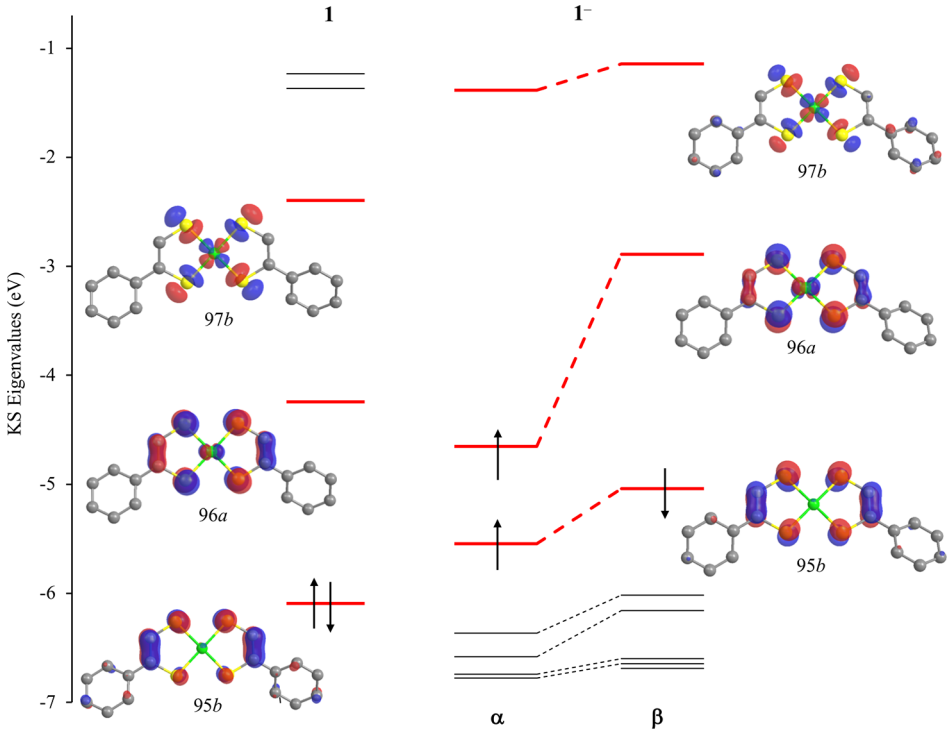

Figure 4. Correlation diagram between the eigenvalues of selected KS-MOs (−7.0/−0.7 eV) calculated for the *cis* isomer of **1** (left) and $\mathbf{1}^-$ (right) in CH_2Cl_2 (IEF-PCM SCRF model), and drawings of the frontier KS-MOs, highlighted in red (C_2 point group; contour value = 0.05 lel).

cally coupled ligands $\mathbf{L}^{\bullet-}$.[80,81] According to the latter view, the redox steps typically exhibited by bis(1,2-dithiolene) complexes of d^8 metal ions (Scheme S1) would be ligand-centered and would not modify the electron population on the central Ni^{II} ion:

$$[Ni^{II}(\mathbf{L}^{2-})_2]^{2-} \rightleftharpoons [Ni^{II}(\mathbf{L}^{2-})(\mathbf{L}^{\bullet-})]^{-} \rightleftharpoons [Ni^{II}(\mathbf{L}^{\bullet-})_2] \quad (2)$$

A series of preliminary calculations were performed on the *cis* isomer of **1** (C_2 point group) in order to ascertain the relative weight of the closed-shell and the diradical descriptions of the singlet ground state (GS). These calculations indicated a composition of the GS made up by about 80% of the closed-shell system, with a contribution from the diradical form of 20%. The neutral complexes **1** and **2** were thus optimized in the predominant closed-shell restricted singlet configuration (^{1}A GS in the C_2 point group). Given the possibility of the complexes to exhibit *cis*/*trans* isomerism, both conformations were optimized for all of the complexes (Tables S3−S10). Solvation calculations in CH_2Cl_2 were also carried out at the same level of theory, by using the integral equation formalism of the polarizable continuous model (IEF-PCM) within the self-consistent reaction field (SCRF) approach,[71] and a comparison between the structures optimized in the gas phase and in CH_2Cl_2 showed negligible differences (Tables S11 and S12 for $\mathbf{1}^{x-}$ and $\mathbf{2}^{x-}$, respectively).

Good agreement was found between the optimized structures (Figure S10 for **1** and **2**) and the corresponding structural data of **1**, **2**, $\mathbf{1}^-$, and $\mathbf{2}^-$ discussed above, only the Ni−S bond distances being slightly overestimated (by less than 0.04 Å). In agreement with structural data, the replacement of the phenyl ring in $\mathbf{1}^{x-}$ with the 2-naphtyl substituent in $\mathbf{2}^{x-}$ does not induce significant modifications in the optimized bond lengths and angles (varying by less than 0.01 Å and 1°, respectively). The *cis*/*trans* isomers were found to differ by less than 0.1 kcal mol^{-1} in their total electronic energies for all of the complexes and very small variations can be observed when their optimized geometries are compared (bond distances and angles differing by less than 0.01 Å and 1°, respectively). In all the optimized structures the aryl substituents are twisted with respect to the central metallacycles by 24.45−29.90° (25.79−30.37° in CH_2Cl_2). A scan of the potential energy surface (PES) was performed by optimizing the geometry of each complex at different frozen values of the corresponding dihedral angle τ ($0° \leq \tau \leq 180°$; C1−C2−C3−C4 in Figure S10), showing that the corresponding rotational barrier is in any case small (3.0−4.4 kcal mol^{-1}; Figure S11 for $\mathbf{1}^{x-}$). It can thus be hypothesized that a free rotation of the aryl substituents occurs in solution and that the differences observed in the crystal structure are probably steered by the solid-state packing. In agreement with the experimental structural data discussed above, neutral complexes **1** and **2** feature C−C and C−S optimized distances that are systematically longer and shorter, respectively, than those of the corresponding monoanions. Moreover, an analysis of the natural charges[72] (Table S13) shows that the nickel charge does not undergo a significant variation on passing from **1** and **2** to $\mathbf{1}^-$ and $\mathbf{2}^-$, respectively (0.060 and 0.006 lel on average in the gas phase and CH_2Cl_2, respectively), thereby further confirming that the corresponding electron-transfer process is mostly ligand-based. An examination of the GS bonding scheme of **1** and **2** shows that the two complexes feature very similar Kohn−Sham molecular orbital (KS-MO) compositions, regardless of the isomerism. In particular, both the highest occupied and lowest unoccupied molecular orbital (HOMO and LUMO, respectively; KS-MOs 95/96 and 121/122 in Figures 4 and S12 for the *cis* conformations of **1** and **2**, respectively, in CH_2Cl_2) are π-MOs mostly localized on the 1,2-dithiolene core, with a minor contribution (7% for **1**; 6%

https://dx.doi.org/10.1021/acs.inorgchem.0c00491
Inorg. Chem. XXXX, XXX, XXX−XXX

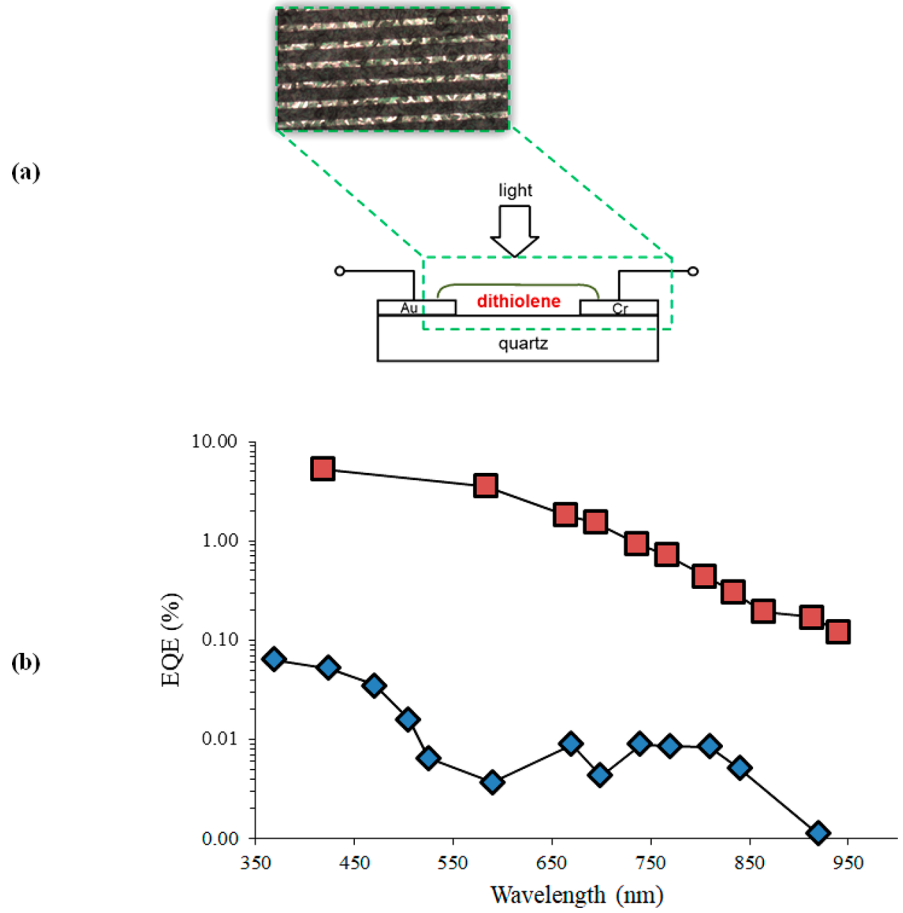

Figure 5. (a) Sketch of the planar photodetector prototype and dark-field optical microscopy image (1000× magnification) of the device based on **1**, showing the complex cast on the lithographed quartz substrate. (b) EQE spectrum recorded for the photoconductive devices based on **1** and **2** (red and blue squares, respectively).

for **2**) from the central nickel ion in the case of the LUMO. In $\mathbf{1}^-$ and $\mathbf{2}^-$ the LUMO is an antibonding σ-MO built up by the combination of the in-plane sulfur 2p atomic orbitals (AOs) with the nickel 3d AO (KS-MOs 97 and 123 in Figures 4 and S12). The localization of the frontier MOs on the 1,2-dithiolene core accounts for the negligible dependence of the experimental redox potentials on the substitution and isomerism of the ligands.

Time-dependent DFT calculations were carried out in CH_2Cl_2 at the optimized geometries in the GS for the *cis* and *trans* isomers of **1**, $\mathbf{1}^-$, **2**, and $\mathbf{2}^-$. Notably, the *cis* and *trans* isomers of the complexes show vis−NIR electronic transitions energies differing by less than 0.03 eV (Table S14). TD-DFT calculations show that for neutral complexes **1** and **2** the intense NIR absorption (calculated at 780 and 845 nm, respectively; Table S14) should be attributed to the S0 → S1 one-electron vertical transition corresponding to an almost pure (94 and 97%, respectively) one-electron excitation between the HOMO and LUMO (KS-MOs 95 and 96 for **1**; 121 and 122 for **2**). In contrast, for $\mathbf{1}^-$ and $\mathbf{2}^-$ the NIR absorption (988 and 1002 nm, respectively) corresponds to the D0 → D4 vertical transition, which can in turn be attributed (82 and 87% for $\mathbf{1}^-$ and $\mathbf{2}^-$, respectively) to the SOMO−1 → SOMO ($95\beta \rightarrow 96\beta$ for $\mathbf{1}^-$; $121\beta \rightarrow 122\beta$ for $\mathbf{2}^-$, Table S14 and Figure S12) one-electron excitation. The lower oscillator strengths f and energies of the NIR transition calculated for $\mathbf{1}^-$ and $\mathbf{2}^-$ (average $f = 0.23$) compared to **1** and **2** (average $f = 0.57$) are consistent with the smaller ε and larger λ_{max} values observed experimentally.

Photoconductivity Measurements. The photoconductive properties of the title complexes were investigated through prototype lateral devices prepared by spraying $CHCl_3$ solutions ($C \approx 1$ mg mL^{-1}) of each complex on a quartz substrate with previously lithographed gold/chromium electrodes with an interelectrode spacing of 6 μm (Figure 5). The devices were kept in vacuum (pressure below 10^{-3} mbar) and irradiated with a set of LEDs emitting a power density of a few mW cm^{-2}. Photodetecting properties were investigated by applying an external bias voltage V_{BIAS}= 60 V and measuring the dc photocurrent by means of a semiconductor parameter analyzer. The applied voltage, besides allowing collection of the photogenerated charge carriers, is crucial in the photocarrier generation process; in fact, in amorphous molecular solids, optical excitations do not directly lead to the generation of free charge carriers since the primary excitations are in the form of strongly bound molecular excitons.[89]

While compounds $(TBA^+)(\mathbf{1}^-)$ and $(TBA^+)(\mathbf{2}^-)$ did not show any photodetecting behavior, neutral complexes **1** and **2** proved to be photoconductive. In agreement with diffuse reflectance spectrophotometric measurements (see above), the devices based on complexes **1** and **2** show a wide spectral responsivity, which extends from the vis to the NIR region of the spectrum, complex **2** showing a larger NIR selectivity of the photoresponse (Figure 5). Interestingly, the observed

https://dx.doi.org/10.1021/acs.inorgchem.0c00491
Inorg. Chem. XXXX, XXX, XXX−XXX

external quantum efficiency (EQE) values (7×10^{-1} and 8×10^{-3}% at 770 nm for **1** and **2**, respectively, Table S15) were found to be about 1−2 orders of magnitude larger than those of analogous devices based on pristine dithiolene materials investigated previously.[41−43]

The differences observed in the photoconductive properties of $(TBA^+)(\mathbf{1}^-−\mathbf{2}^-)$ and **1**−**2** might be possibly attributed to differences in their solid-state packing.[90−93] In this context, the lack of photoconductivity of the monoanionic complexes could be ascribed to the presence of the bulky TBA^+ counter-cations, which in the solid state interpose between the complex molecules as described above. In contrast, in the case of complexes **1** and **2** the possibility of neighboring molecules to interact through S···S and Ni···S contacts, evidenced in the crystal structures, may allow for an electron-hopping process responsible for the photoinduced conductivity. This notwithstanding, the deposition process results in an amorphous deposition on the device. Thus, the effective solid-state intermolecular interactions as well as the balance between the *cis* and *trans* isomers are unknown, and fine differences might be responsible for the larger efficiency observed for complex **1** with respect to that for complex **2**.

CONCLUSIONS

In conclusion, metal bis(1,2-dithiolene) complexes belonging to the class $[Ni(Ar\text{-}edt)_2]^{x-}$ (Ar = phenyl, 2-naphthyl; x = 0 and 1) represent promising active materials for optoelectronic applications, and air-stable prototype photodetectors sensitive to the NIR region of the spectrum have been developed based on these systems. Several factors render these devices appealing for telecommunication. First, metal 1,2-dithiolene complexes feature high thermal and photochemical stability,[1−3] uncommon among photoactive organic materials showing low HOMO−LUMO energy gaps.[43,94] In addition, the possibility to deposit the active complexes on substrates of any extension and shape allows for applications precluded to inorganic semiconductors. Finally, the possibility of casting the complexes from organic solvents enables the fabrication of devices directly on the surface of optical elements, such as beam splitters and fiber-optical-cleaved surfaces, solving alignment problems at the root.

Importantly, EQE values orders of magnitude higher than those of analogous devices based on pristine dithiolene materials were recorded, representing a great step forward in solving the previously encountered limitations represented by low quantum efficiency. Significant variations in the photoresponse were observed upon modifying both the oxidation state of the complexes and the substituents at the ligands.

Since photoconductivity is dependent on the number of the photogenerated electron−hole pairs and the mobility of the carriers,[95] the larger efficiency of $[Ni(Ar\text{-}edt)_2]$ metal bis(1,2-dithiolene) complexes with respect to those reported in the past,[39−43] as well as the differences between **1** and **2**, can be tentatively attributed to the their different solid-state structures, given the extreme sensitivity of the solid-state electronic properties of molecular materials to minute changes of the molecular shapes and intermolecular interactions. Future studies will be directed at addressing these aspects.

ASSOCIATED CONTENT

Supporting Information

The Supporting Information is available free of charge at https://pubs.acs.org/doi/10.1021/acs.inorgchem.0c00491.

Crystallographic data and packing details for 4-phenyl-[1,3]dithiol-2-one, **1**, **2**, $(TBA^+)(\mathbf{1}^-)$, and $(TBA^+)(\mathbf{2}^-)$; ^{1}H NMR spectrum of **1**; CV data for $(TBA^+)(\mathbf{1}^-)$ and $(TBA^+)(\mathbf{2}^-)$; absorption UV−vis−NIR spectra of $(TBA^+)(\mathbf{1}^-)$, $(TBA^+)(\mathbf{2}^-)$, **1**, and **2**; diffuse reflectance spectra for **1** and **2**; DFT-optimized geometries and relative metric parameters, NBO charges, and TD-DFT data for $\mathbf{1}^{x-}$ and $\mathbf{2}^{x-}$; PES surfaces for $\mathbf{1}^{x-}$; KS-MOs drawings and correlation diagram for $\mathbf{2}^{x-}$; photoconductivity data for **1** and **2** (x = 0 and 1) (PDF)

Accession Codes

CCDC 1953275−1953278 contain the supplementary crystallographic data for this paper. These data can be obtained free of charge via www.ccdc.cam.ac.uk/data_request/cif, or by emailing data_request@ccdc.cam.ac.uk, or by contacting The Cambridge Crystallographic Data Centre, 12 Union Road, Cambridge CB2 1EZ, UK; fax: +44 1223 336033.

AUTHOR INFORMATION

Corresponding Authors

Anna Pintus − *Università degli Studi di Cagliari, Dipartimento di Scienze Chimiche e Geologiche, 09042 Monserrato (Cagliari), Italy;* orcid.org/0000-0001-6069-9771; Email: apintus@unica.it

Massimiliano Arca − *Università degli Studi di Cagliari, Dipartimento di Scienze Chimiche e Geologiche, 09042 Monserrato (Cagliari), Italy;* orcid.org/0000-0002-0058-6406; Email: marca@unica.it

Authors

Lucia Ambrosio − *Università degli Studi di Cagliari, Dipartimento di Scienze Chimiche e Geologiche, 09042 Monserrato (Cagliari), Italy*

M. Carla Aragoni − *Università degli Studi di Cagliari, Dipartimento di Scienze Chimiche e Geologiche, 09042 Monserrato (Cagliari), Italy;* orcid.org/0000-0002-5010-7370

Maddalena Binda − *Center for Nano Science and Technology @ Polimi, Istituto Italiano di Tecnologia, 20133 Milano, Italy*

Simon J. Coles − *UK National Crystallography Service, School of Chemistry, Faculty of Engineering and Physical Sciences, University of Southampton, SO17 1BJ Southampton, United Kingdom;* orcid.org/0000-0001-8414-9272

Michael B. Hursthouse − *UK National Crystallography Service, School of Chemistry, Faculty of Engineering and Physical Sciences, University of Southampton, SO17 1BJ Southampton, United Kingdom*

Francesco Isaia − *Università degli Studi di Cagliari, Dipartimento di Scienze Chimiche e Geologiche, 09042 Monserrato (Cagliari), Italy;* orcid.org/0000-0003-2139-8188

Vito Lippolis − *Università degli Studi di Cagliari, Dipartimento di Scienze Chimiche e Geologiche, 09042 Monserrato (Cagliari), Italy;* orcid.org/0000-0001-8093-576X

Giammarco Meloni − *Università degli Studi di Cagliari, Dipartimento di Scienze Chimiche e Geologiche, 09042 Monserrato (Cagliari), Italy*

Dario Natali − *Center for Nano Science and Technology @ Polimi, Istituto Italiano di Tecnologia, 20133 Milano, Italy; Politecnico di Milano, Dipartimento di Elettronica, Informazione e Bioingegneria, 20133 Milano, Italy;* orcid.org/0000-0003-3535-3490

James B. Orton − *UK National Crystallography Service, School of Chemistry, Faculty of Engineering and Physical Sciences, University of Southampton, SO17 1BJ Southampton, United Kingdom*

Enrico Podda − *Università degli Studi di Cagliari, Dipartimento di Scienze Chimiche e Geologiche, 09042 Monserrato (Cagliari), Italy;* orcid.org/0000-0002-4329-7751

Marco Sampietro − *Center for Nano Science and Technology @ Polimi, Istituto Italiano di Tecnologia, 20133 Milano, Italy; Politecnico di Milano, Dipartimento di Elettronica, Informazione e Bioingegneria, 20133 Milano, Italy;* orcid.org/0000-0003-4825-9612

Complete contact information is available at: https://pubs.acs.org/10.1021/acs.inorgchem.0c00491

Author Contributions

The manuscript was written through contributions of all authors. All authors have given approval to the final version of the manuscript.

Notes

The authors declare no competing financial interest.

■ ACKNOWLEDGMENTS

M.A., M.C.A., F.I., and V.L. thank the Fondazione di Sardegna (FdS) and Regione Autonoma della Sardegna (RAS) (Progetti Biennali di Ateneo FdS/RAS annualità 2016) for financial support. A.P. acknowledges RAS for the funding in the context of the POR FSE 2014−2020 (CUP F24J17000190009). S.J.C. and J.B.O. would thank the UK Engineering and Physical Sciences Research Council for their continued support for the National Crystallography Service (NCS), based at the University of Southampton, UK.

■ DEDICATION

Dedicated to Prof. Francesco A. Devillanova in occasion of his 81st birthday.

■ REFERENCES

(1) McCleverty, J. A. Metal 1, 2-dithiolene and related complexes. *Prog. Inorg. Chem.* **2007**, *10*, 49−221.

(2) (a) Stiefel, E. I., Ed. *Dithiolene Chemistry: Synthesis, Properties, and Applications*; Wiley: Hoboken, 2004. (b) Arca, M.; Aragoni, M. C.; Pintus, A. In *Handbook of Chalcogen Chemistry*; Devillanova, F. A., du Mont, W.-W., Eds.; RSC Publishing: Cambridge, 2013; pp 127−179.

(3) (a) Robertson, N.; Cronin, L. Metal bis-1,2-dithiolene complexes in conducting or magnetic crystalline assemblies. *Coord. Chem. Rev.* **2002**, *227*, 93−127. (b) Kobayashi, A.; Fujiwara, E.; Kobayashi, H. Single-Component Molecular Metals with Extended-TTF Dithiolate Ligands. *Chem. Rev.* **2004**, *104*, 5243−5264. (c) Kato, R. Conducting metal dithiolene complexes: Structural and electronic properties. *Chem. Rev.* **2004**, *104*, 5319−5346. (d) Faulmann, C.; Cassoux, P. Electrical conductivity and spin crossover: A new achievement with a metal bis dithiolene complex. *Prog. Inorg. Chem.* **2004**, *52*, 399−489. (e) Wang, K. Electrochemical and chemical reactivity of dithiolene complexes. *Prog. Inorg. Chem.* **2004**, *52*, 267−314. (f) Beswick, C. L.; Schulman, J. A.; Stiefel, E. I. Structures and structural trends in homoleptic dithiolene complexes. *Prog. Inorg. Chem.* **2004**, *52*, 55−110. (g) Kirk, M. L.; McNaughton, R. L.; Helton, M. E. The electronic structure and spectroscopy of metallo-dithiolene complexes. *Prog. Inorg. Chem.* **2004**, *52*, 111−212. (h) Cummings, S. D.; Eisenberg, R. Luminescence and Photochemistry of Metal Dithiolene Complexes. *Prog. Inorg. Chem.* **2004**, *52*, 315−367.

(4) (a) Hine, F. J.; Taylor, A. J.; Garner, C. D. Dithiolene complexes and the nature of molybdopterin. *Coord. Chem. Rev.* **2010**, *254*, 1570−1579. (b) Rabaça, S.; Almeida, M. Dithiolene complexes containing N coordinating groups and corresponding tetrathiafulvalene donors. *Coord. Chem. Rev.* **2010**, *254*, 1493−1508. (c) Garreau-de Bonneval, B.; Moineau-Chane Ching, K. I.; Alary, F.; Bui, T.-T.; Valade, L. Neutral d^8 metal bis-dithiolene complexes: synthesis, electronic properties and applications. *Coord. Chem. Rev.* **2010**, *254*, 1457−1467. (d) Dalgleish, S.; Robertson, N. Electropolymerisable dithiolene complexes. *Coord. Chem. Rev.* **2010**, *254*, 1549−1558. (e) Mitsopoulou, C. A. Identifying of charge-transfer transitions and reactive centers in M(diimine)(dithiolate) complexes by DFT techniques. *Coord. Chem. Rev.* **2010**, *254*, 1448−1456.

(5) (a) Sproules, S.; Wieghardt, K. Dithiolene radicals: Sulfur K-edge X-ray absorption spectroscopy and Harry's intuition. *Coord. Chem. Rev.* **2011**, *255*, 837−860. (b) Zarkadoulas, A.; Koutsouri, E.; Mitsopoulou, C. A. A perspective on solar energy conversion and water photosplitting by dithiolene complexes. *Coord. Chem. Rev.* **2012**, *256*, 2424−2434. (c) Sproules, S. Tris(dithiolene) chemistry: A golden jubilee. *Prog. Inorg. Chem.* **2014**, *58*, 1−144.

(6) Leimkuhler, S. Shared function and moonlighting proteins in molybdenum cofactor biosynthesis. *Biol. Chem.* **2017**, *398*, 1009−1026.

(7) Holm, R. H.; Kennepohl, P.; Solomon, E. I. Structural and functional aspects of metal sites in biology. *Chem. Rev.* **1996**, *96*, 2239−2314.

(8) Liu, Y.; Zhang, Z.; Chen, X.; Xu, S.; Cao, S. Near-infrared absorbing dyes at 1064 nm: Soluble dithiolene nickel complexes with alkylated electron-donating groups as Peripheral substituents. *Dyes Pigm.* **2016**, *128*, 179−189.

(9) Chatzikyriakos, G.; Papagiannouli, I.; Couris, S.; Anyfantis, G.C.; Papavassiliou, G.C. Nonlinear optical response of a symmetrical Au dithiolene complex under ps and ns laser excitation in the infrared and in the visible. *Chem. Phys. Lett.* **2011**, *513*, 229−235.

(10) Guo, W. F.; Sun, X. B.; Sun, J.; Wang, X. Q.; Zhang, G. H.; Ren, Q.; Xu, D. Nonlinear optical absorption of a metal dithiolene complex irradiated by different laser pulses at near-infrared wavelengths. *Chem. Phys. Lett.* **2007**, *435*, 65−68.

(11) Cassano, T.; Tommasi, R.; Nitti, L.; Aragoni, M. C.; Arca, M.; Denotti, C.; Devillanova, F. A.; Isaia, F.; Lippolis, V.; Lelj, F.; Romaniello, P. Picosecond absorption saturation dynamics in neutral $[M(R, R'timdt)_2]$ metal-dithiolenes. *J. Chem. Phys.* **2003**, *118*, 5995−6002.

(12) Mueller-Westerhoff, U. T.; Vance, B.; Ihl Yoon, D. The synthesis of dithiolene dyes with strong near-IR absorption. *Tetrahedron* **1991**, *47*, 909−932.

(13) Nunes, J.; Figueira, M.; Belo, D.; Santos, I.; Ribeiro, B.; Lopes, E.; Henriques, R.; Vidal-Gancedo, J.; Veciana, J.; Rovira, C.; Almeida, M. Transition Metal Bisdithiolene Complexes Based on Extended Ligands with Fused Tetrathiafulvalene and Thiophene Moieties: New Single-Component Molecular Metals. *Chem. - Eur. J.* **2007**, *13*, 9841−9849.

(14) McNamara, W.; Han, Z.; Yin, C.-J.; Brennessel, W. W.; Holland, P. L.; Eisenberg, R. Cobalt-dithiolene complexes for the photocatalytic and electrocatalytic reduction of protons in aqueous solutions. *Proc. Natl. Acad. Sci. U. S. A.* **2012**, *109*, 15594−15599.

(15) Wang, K.; Stiefel, E. I. Toward separation and purification of olefins using dithiolene complexes: An electrochemical approach. *Science* **2001**, *291*, 106−109.

(16) Barriere, F.; Camire, N.; Geiger, W. E.; Mueller-Westerhoff, U. T.; Sanders, R. Use of Medium Effects to Tune the $\Delta E_{1/2}$ Values of Bimetallic and Oligometallic Compounds. *J. Am. Chem. Soc.* **2002**, *124*, 7262−7263.

(17) Lim, B. S.; Fomitchev, D. V.; Holm, R. H. Nickel Dithiolenes Revisited: Structures and Electron Distribution from Density Functional Theory for the Three-Member Electron-Transfer Series $[Ni(S_2C_2Me_2)_2]^{0,1-,2-}$. *Inorg. Chem.* **2001**, *40*, 4257−4262.

(18) Chirik, P. J. Preface: forum on redox-active ligands. *Inorg. Chem.* **2011**, *50*, 9737−9740.

https://dx.doi.org/10.1021/acs.inorgchem.0c00491
Inorg. Chem. XXXX, XXX, XXX−XXX

(19) Allwright, E.; Silber, G.; Crain, J.; Matsushita, M. M.; Awaga, K.; Robertson, N. Electrochemical deposition of highly-conducting metal dithiolene films. *Dalton Trans.* **2016**, *45*, 9363−9368.
(20) Amb, C. M.; Heth, C. L.; Evenson, S. J.; Pokhodnya, K. I.; Rasmussen, S. C. Thiophene-Fused Nickel Dithiolenes: A Synthetic Scaffold for Highly Delocalized π-Electron Systems. *Inorg. Chem.* **2016**, *55*, 10978−10989.
(21) Miao, Q. Q.; Gao, J. X.; Wang, Z. Q.; Yu, H.; Luo, Y.; Ma, T. L. Syntheses and characterization of several nickel bis(dithiolene) complexes with strong and broad Near-IR absorption. *Inorg. Chim. Acta* **2011**, *376*, 619−627.
(22) Eisenberg, R.; Gray, H. B. Noninnocence in metal complexes: A dithiolene dawn. *Inorg. Chem.* **2011**, *50*, 9741−9751.
(23) Sun, L.; Shu, S.; Zhou, Y.; Hou, S.; Liu, Y.; Ke, Z. Regulating the Optoelectronic Properties of Nickel Dithiolene by the Substituents: A Theoretical Study. *Materials* **2018**, *11*, 2192−2203.
(24) Qu, L.; Guo, Y.; Luo, H.; Zhong, C.; Yu, G.; Liu, Y.; Qin, J. A simple nickel bis(dithiolene) complex as an excellent n-type molecular semiconductor for field-effect transistors. *Chem. Commun.* **2012**, *48*, 9965−9967.
(25) Wada, H.; Taguchi, T.; Noda, B.; Kambayashi, T.; Mori, T.; Ishikawa, K.; Takezoe, H. Air stability of n-channel organic transistors based on nickel coordination compounds. *Org. Electron.* **2007**, *8*, 759−766.
(26) Huong, V. T. T.; Tai, T. B.; Nguyen, M. T. A theoretical study on charge transport of dithiolene nickel complexes. *Phys. Chem. Chem. Phys.* **2016**, *18*, 6259−6267.
(27) Nguyen, H. T.; Nguyen, M. T. Silole-based nickel bisdithiolene complexes: A theoretical design for optoelectronic applications. *J. Phys. Chem. C* **2016**, *120*, 16418−16426.
(28) Charrier, D. S. H.; de Vries, T.; Mathijssen, S. G. J.; Geluk, E. J.; Smits, E. C. P.; Kemerink, M.; Janssen, R. A. J. Bimolecular recombination in ambipolar organic field effect transistors. *Org. Electron.* **2009**, *10*, 994−997.
(29) Anthopoulos, T. D.; Anyfantis, G. C.; Papavassiliou, G. C.; de Leeuw, D. M. Air-stable ambipolar organic transistors. *Appl. Phys. Lett.* **2007**, *90*, 122105.
(30) Dalgleish, S.; Labram, J. G.; Li, Z.; Wang, J.; McNeill, C. R.; Anthopoulos, T. D.; Greenham, N. C.; Robertson, N. Indole-substituted nickel dithiolene complexes in electronic and optoelectronic devices. *J. Mater. Chem.* **2011**, *21*, 15422−15430.
(31) Aloukos, P.; Couris, S.; Koutselas, J. B.; Anyfantis, G. C.; Papavassiliou, G. C. Transient nonlinear optical response of novel neutral unsymmetrical nickel dithiolene complexes. *Chem. Phys. Lett.* **2006**, *428*, 109−113.
(32) Iliopoulos, K.; El-Ghayoury, A.; Derkowska, B.; Ranganathan, A.; Batail, P.; Gindre, D.; Sahraoui, B. Effect of metal cation complexation on the nonlinear optical response of an electroactive bisiminopyridine ligand. *Appl. Phys. Lett.* **2012**, *101*, 261105.
(33) Majumder, M.; Misra, A. Strategic design of thiophene-fused nickel dithiolene derivatives for efficient NLO response. *Phys. Chem. Chem. Phys.* **2018**, *20*, 19007−19016.
(34) Avramopoulos, A.; Reis, H.; Otero, N.; Karamanis, P.; Pouchan, C.; Papadopoulos, M. G. A series of novel derivatives with giant second hyperpolarizabilities, based on radiaannulenes, tetrathiafulvalene, nickel dithiolene, and their lithiated analogues. *J. Phys. Chem. C* **2016**, *120*, 9419−9435.
(35) Marshall, K. L.; Painter, G.; Lotito, K.; Noto, A. G.; Chang, P. Transition metal dithiolene near-IR dyes and their applications in liquid crystal devices. *Mol. Cryst. Liq. Cryst.* **2006**, *454*, 47.
(36) Shen, W.-C.; Huo, P.; Huang, Y.-D.; Yin, J.-X.; Zhu, Q.-Y.; Dai, J. Photocurrent responsive films prepared from a nickel-dithiolate compound with directly bonded pyridyl groups. *RSC Adv.* **2014**, *4*, 60221−60226.
(37) Naito, T.; Karasudani, T.; Nagayama, N.; Ohara, K.; Konishi, K.; Mori, S.; Takano, T.; Takahashi, Y.; Inabe, T.; Kinose, S.; Nishihara, S.; Inoue, K. Giant Photoconductivity in NMQ[Ni(dmit)$_2$]. *Eur. J. Inorg. Chem.* **2014**, *2014*, 4000−4009.
(38) Dalgleish, S.; Matsushita, M. M.; Hu, L.; Li, B.; Yoshikawa, H.; Awaga, K. Utilizing photocurrent transients for dithiolene-based photodetection: stepwise improvements at communications relevant wavelengths. *J. Am. Chem. Soc.* **2012**, *134*, 12742−12750.
(39) Aragoni, M. C.; Arca, M.; Cassano, T.; Denotti, C.; Devillanova, F. A.; Isaia, F.; Lippolis, V.; Natali, D.; Nitti, L.; Sampietro, M.; Tommasi, R.; Verani, G. Photoinduced conductivity and nonlinear optical properties of [M(R, R′ timdt)$_2$] dithiolenes (M = Ni, Pd, Pt; R, R′ timdt = monoreduced imidazolidine-2,4,5-trithione) as materials for optically driven switches and photodetectors. *Inorg. Chem. Commun.* **2002**, *5*, 869−872.
(40) Natali, D.; Sampietro, M.; Arca, M.; Denotti, C.; Devillanova, F. A. Wavelength-selective organic photodetectors for near-infrared applications based on novel neutral dithiolenes. *Synth. Met.* **2003**, *137*, 1489−1490.
(41) Aragoni, M. C.; Arca, M.; Devillanova, F. A.; Isaia, F.; Lippolis, V.; Mancini, A.; Pala, L.; Verani, G.; Agostinelli, T.; Caironi, M.; Natali, D.; Sampietro, M. First example of a near-IR photodetector based on neutral [M(R-dmet)$_2$] bis(1, 2-dithiolene) metal complexes. *Inorg. Chem. Commun.* **2007**, *10*, 191−194.
(42) Aragoni, M. C.; Arca, M.; Caironi, M.; Denotti, C.; Devillanova, F. A.; Grigiotti, E.; Isaia, F.; Laschi, F.; Lippolis, V.; Natali, D.; Pala, L.; Sampietro, M.; Zanello, P. Monoreduced [M(R, R′timdt)$_2$]$^-$ dithiolenes (M = Ni, Pd, Pt; R, R′timdt = disubstituted imidazolidine-2,4,5-trithione): solid state photoconducting properties in the third optical fiber window. *Chem. Commun.* **2004**, 1882−1883.
(43) Caironi, M.; Natali, D.; Sampietro, M.; Ward, M.; Meacham, A.; Devillanova, F. A.; Arca, M.; Denotti, C.; Pala, L. Near infrared detection by means of coordination complexes. *Synth. Met.* **2005**, *153*, 273−276.
(44) Sugimori, A.; Tachiya, N.; Kajitani, M.; Akiyama, T. Radical Substitution in the Nickeladithiolene Ring in Bis(1-phenyl-1,2-ethenedithiolato)nickel(0). *Organometallics* **1996**, *15*, 5664−5668.
(45) Madhu, V.; Das, S. K. New series of asymmetrically substituted bis(1,2-dithiolato)-nickel (III) complexes exhibiting near IR absorption and structural diversity. *Inorg. Chem.* **2008**, *47*, 5055−5070.
(46) Vuong, T. M. H.; Bui, T.-T.; Sournia-Saquet, A.; Moreau, A.; Ching, K. I. M.-C. Heteroleptic Bis(cis-1,2-disubstituted ethylene-1,2-dithiolato)nickel Complexes Obtained by Ligand-Exchange Reaction: Synthesis and Properties. *Inorg. Chem.* **2014**, *53*, 2841−2847.
(47) Ghosh, A. C.; Weisz, K.; Schulzke, C. Selective Capture of Ni^{2+} Ions by Naphthalene- and Coumarin-Substituted Dithiolenes. *Eur. J. Inorg. Chem.* **2016**, *2016*, 208−218.
(48) Ambrosio, L.; Aragoni, M. C.; Arca, M.; Devillanova, F. A.; Hursthouse, M. B.; Huth, S. L.; Isaia, F.; Lippolis, V.; Mancini, A.; Pintus, A. Synthesis and Characterization of Novel Gold(III) Complexes of Asymmetrically Aryl-Substituted 1,2-Dithiolene Ligands Featuring Potential-Controlled Spectroscopic Properties. *Chem. - Asian J.* **2010**, *5*, 1395−1406.
(49) Aragoni, M. C.; Arca, M.; Devillanova, F. A.; Isaia, F.; Lippolis, V.; Pintus, A. Gold(III) Complexes of Asymmetrically Aryl-Substituted 1,2-Dithiolene Ligands Featuring Potential-Controlled Spectroscopic Properties: An Insight into the Electronic Properties of bis(Pyren-1-yl-ethylene-1,2-dithiolato)Gold(III). *Chem. - Asian J.* **2011**, *6*, 198−208.
(50) Otwinowski, Z.; Minor, W. Processing of X-ray diffraction data collected in oscillation mode. *Methods Enzymol.* **1997**, *276*, 307−326.
(51) Hooft, R. W. *COLLECT*; Nonius BV: Delft, The Netherlands, 1998.
(52) Sheldrick, G. M.; *SHELXS-97, Program for Crystal Structure Solution*; University of Göttingen: Gottingen, Germany, 1997.
(53) Sheldrick, G. M.; *SHELXL-97, Program for X-ray Crystal Structure Refinement*; University of Göttingen: Germany, 1997.
(54) *Rigaku Crystal Clear-SM Expert, Software For Data Collection and Processing*, version 3.1 b22; Rigaku Corporation: Tokyo, Japan, 2011.
(55) Farrugia, L. J. WinGX and ORTEP for Windows: an update. *J. Appl. Crystallogr.* **2012**, *45*, 849−854.

https://dx.doi.org/10.1021/acs.inorgchem.0c00491
Inorg. Chem. XXXX, XXX, XXX−XXX

(56) *CrysAlisPro Software System*; Rigaku Oxford Diffraction: The Woodlands, TX, 2019.
(57) Sheldrick, G. M. SHELXT − Integrated space-group and crystal-structure determination. *Acta Crystallogr., Sect. A: Found. Adv.* **2015**, *A71*, 3−8.
(58) Dolomanov, O. V.; Bourhis, L. J.; Gildea, R. J.; Howard, J. A. K.; Puschmann, H. OLEX2: a complete structure solution, refinement and analysis program. *J. Appl. Crystallogr.* **2009**, *42*, 339−341.
(59) Sheldrick, G. M. Crystal structure refinement with SHELXL. *Acta Crystallogr., Sect. C: Struct. Chem.* **2015**, *C71*, 3−8.
(60) *SAINT*, version 6.02a; Bruker AXS Inc.: Madison, WI, 2000.
(61) *SADABS*, version 2.03; Bruker AXS Inc.: Madison, WI, 2000.
(62) Koch, W.; Holthausen, M. C. *A Chemist's Guide to Density Functional Theory*, 2nd ed.; Wiley-VCH: Weinheim, 2002.
(63) Frisch, M. J.; Trucks, G. W.; Schlegel, H. B.; Scuseria, G. E.; Robb, M. A.; Cheeseman, J. R.; Scalmani, G.; Barone, V.; Petersson, G. A.; Nakatsuji, H.; Li, X.; Caricato, M.; Marenich, A. V.; Bloino, J.; Janesko, B. G.; Gomperts, R.; Mennucci, B.; Hratchian, H. P.; Ortiz, J. V.; Izmaylov, A. F.; Sonnenberg, J. L.; Williams-Young, D.; Ding, F.; Lipparini, F.; Egidi, F.; Goings, J.; Peng, B.; Petrone, A.; Henderson, T.; Ranasinghe, D.; Zakrzewski, V. G.; Gao, J.; Rega, N.; Zheng, G.; Liang, W.; Hada, M.; Ehara, M.; Toyota, K.; Fukuda, R.; Hasegawa, J.; Ishida, M.; Nakajima, T.; Honda, Y.; Kitao, O.; Nakai, H.; Vreven, T.; Throssell, K.; Montgomery, J. A., Jr.; Peralta, J. E.; Ogliaro, F.; Bearpark, M.; Heyd, J. J.; Brothers, E. N.; Kudin, K. N.; Staroverov, V. N.; Kobayashi, R.; Normand, J.; Raghavachari, K.; Rendell, A.; Burant, J. C.; Iyengar, S. S.; Tomasi, J.; Cossi, M.; Millam, J. M.; Klene, M.; Adamo, C.; Cammi, R.; Ochterski, J. W.; Martin, R. L.; Morokuma, K.; Farkas, O.; Foresman, J. B.; Fox, D. J. *Gaussian 16*, revision B.01; Gaussian, Inc.: Wallingford CT, 2016.
(64) Adamo, C.; Barone, V. Exchange functionals with improved long-range behavior and adiabatic connection methods without adjustable parameters: The mPW and mPW1PW models. *J. Chem. Phys.* **1998**, *108*, 664−75.
(65) Schäfer, A.; Horn, H.; Ahlrichs, R. Fully optimized contracted Gaussian basis sets for atoms Li to Kr. *J. Chem. Phys.* **1992**, *97*, 2571−2577.
(66) Weigend, F.; Ahlrichs, R. Balanced basis sets of split valence, triple zeta valence and quadruple zeta valence quality for H to Rn: Design and assessment of accuracy. *Phys. Chem. Chem. Phys.* **2005**, *7*, 3297−3305.
(67) Roy, L. E.; Hay, J. P.; Martin, L. R. Revised basis sets for the LANL effective core potentials. *J. Chem. Theory Comput.* **2008**, *4*, 1029−1031.
(68) Dunning, T. H., Jr.; Hay, P. J. In *Methods of Electronic Structure Theory*; Schaefer, H. F., III, Ed.: Plenum Press: New York, 1977; Vol. *2*
(69) Schuchardt, K. L.; Didier, B. T.; Elsethagen, T.; Sun, L.; Gurumoorthi, V.; Chase, J.; Li, J.; Windus, T. L. Basis set exchange: a community database for computational sciences. *J. Chem. Inf. Model.* **2007**, *47*, 1045−1052.
(70) Bachler, V.; Olbrich, G.; Neese, F.; Wieghardt, K. Theoretical Evidence for the Singlet Diradical Character of Square Planar Nickel Complexes Containing Two o-Semiquinonato Type Ligands. *Inorg. Chem.* **2002**, *41*, 4179−4193.
(71) Tomasi, J.; Mennucci, B.; Cammi, R. Quantum mechanical continuum solvation models. *Chem. Rev.* **2005**, *105*, 2999−3094.
(72) Reed, A. E.; Weinstock, R. B.; Weinhold, F. Natural population analysis. *J. Chem. Phys.* **1985**, *83*, 735−746.
(73) Dennington, R.; Keith, T. A.; Millam, J. M.; *GaussView*, version 6; Semichem Inc.: Shawnee Mission, KS, 2016.
(74) Schaftenaar, G.; Noordik, J. H. Molden: a pre-and post-processing program for molecular and electronic structures. *J. Comput.-Aided Mol. Des.* **2000**, *14*, 123−134.
(75) Chemissian. http://www.chemissian.com.
(76) O'Boyle, N. M.; Tenderholt, A. L.; Langner, K. M. Cclib: a library for package-independent computational chemistry algorithms. *J. Comput. Chem.* **2008**, *29*, 839−845.
(77) Rauchfuss, T. B. Synthesis of transition metal dithiolenes. *Prog. Inorg. Chem.* **2004**, *52*, 1−54.
(78) Davies, E. S.; Beddoes, R. L.; Collison, D.; Dinsmore, A.; Docrat, A.; Joule, J. A.; Wilson, C. R.; Garner, C. D. Synthesis of oxomolybdenum bis(dithiolene) complexes related to the cofactor of the oxomolybdoenzymes. *J. Chem. Soc., Dalton Trans.* **1997**, 3985−3995.
(79) Mueller-Westerhoff, U. T.; Nazzal, A.; Cox, R. J.; Giroud, A. M. Mesomorphic Transition Metal Complexes. 4. Dithiene Complexes of Ni, Pd, and Pt. *Mol. Cryst. Liq. Cryst.* **1980**, *56*, 249−255.
(80) Ray, K.; Weyhermüller, T.; Neese, F.; Wieghardt, K. Electronic Structure of Square Planar Bis(benzene-1,2-dithiolato)metal Complexes $[M(L)_2]^z$ (z = 2-, 1-, 0; M = Ni, Pd, Pt, Cu, Au): An Experimental, Density Functional, and Correlated ab Initio Study. *Inorg. Chem.* **2005**, *44*, 5345−5360.
(81) Ray, K.; DeBeer George, S.; Solomon, E. I.; Wieghardt, K.; Neese, F. Description of the Ground-State Covalencies of the Bis(dithiolato) Transition-Metal Complexes from X-ray Absorption Spectroscopy and Time-Dependent Density-Functional Calculations. *Chem. - Eur. J.* **2007**, *13*, 2783−2797.
(82) Aragoni, M. C.; Arca, M.; Demartin, F.; Devillanova, F. A.; Garau, A.; Isaia, F.; Lippolis, V.; Verani, G. DFT calculations, structural and spectroscopic studies on the products formed between IBr and N, N′-dimethylbenzoimidazole-2(3H)-thione and −2(3H)-selone. *Dalton Trans.* **2005**, 2252−2258.
(83) Pintus, A.; Aragoni, M. C.; Isaia, F.; Lippolis, V.; Lorcy, D.; Slawin, A. M. Z.; Woollins, J. D.; Arca, M. On the Role of Chalcogen Donor Atoms in Diimine-Dichalcogenolate Pt^{II} SONLO Chromophores: Is It Worth Replacing Sulfur with Selenium? *Eur. J. Inorg. Chem.* **2015**, *2015*, 5163−5170.
(84) Deiana, C.; Aragoni, M. C.; Isaia, F.; Lippolis, V.; Pintus, A.; Slawin, A. M. Z.; Woollins, J. D.; Arca, M. Structural tailoring of the NIR-absorption of bis(1,2-dichalcogenolene) Ni/Pt electrochromophores deriving from 1,3-dimethyl-2-chalcogenoxo-imidazoline-4,5-dichalcogenolates. *New J. Chem.* **2016**, *40*, 8206−8210.
(85) Pintus, A.; Aragoni, M. C.; Coles, S. J.; Coles, S. L.; Isaia, F.; Lippolis, V.; Musteti, A.-M.; Teixidor, F.; Vinas, C.; Arca, M. New Pt ^{II} diimine−dithiolate complexes containing a 1,2-dithiolate-1,2-closo-dicarbadodecarborane: an experimental and theoretical investigation. *Dalton Trans.* **2014**, *43*, 13649−13660.
(86) Pintus, A.; Aragoni, M. C.; Bellec, N.; Devillanova, F. A.; Lorcy, D.; Isaia, F.; Lippolis, V.; Randall, R. A. M.; Roisnel, T.; Slawin, A. M. Z.; Woollins, J. D.; Arca, M. Structure−Property Relationships in Pt^{II} Diimine-Dithiolate Nonlinear Optical Chromophores Based on Arylethylene-1,2-dithiolate and 2-Thioxothiazoline-4,5-dithiolate. *Eur. J. Inorg. Chem.* **2012**, *2012*, 3577−3594.
(87) Periyasamy, G.; Burton, N. A.; Hillier, I. H.; Vincent, M. A.; Disley, H.; McMaster, J.; Garner, C. D. The dithiolene ligand-'innocent' or 'non-innocent'? A theoretical and experimental study of some cobalt-dithiolene complexes. *Faraday Discuss.* **2007**, *135*, 469−488.
(88) Wang, Y.; Xie, Y.; Wei, P.; Schaefer, H. F., III; Robinson, G. H. Redox chemistry of an anionic dithiolene radical. *Dalton Trans.* **2019**, *48*, 3543−3546.
(89) Arkhipov, V. I.; Bässler, H. Exciton dissociation and charge photogeneration in pristine and doped conjugated polymers. *Phys. Stat. Sol. (a)* **2004**, *201*, 1152−1187.
(90) Nan, G.; Shi, Q.; Shuai, Z.; Li, Z. Influences of molecular packing on the charge mobility of organic semiconductors: from quantum charge transfer rate theory beyond the first-order perturbation. *Phys. Chem. Chem. Phys.* **2011**, *13*, 9736−9746.
(91) Campbell, J. E.; Yang, J.; Day, G. M. Predicted energy−structure−function maps for the evaluation of small molecule organic semiconductors. *J. Mater. Chem. C* **2017**, *5*, 7574−7584.
(92) Paudel, K.; Giesbers, G.; Van Schenck, J.; Anthony, J. E.; Ostroverkhova, O. Molecular packing-dependent photoconductivity in functionalized anthradithiophene crystals. *Org. Electron.* **2019**, *67*, 311−319.

https://dx.doi.org/10.1021/acs.inorgchem.0c00491
Inorg. Chem. XXXX, XXX, XXX−XXX

(93) Ionescu, A.; Lento, R.; Mastropietro, T. F.; Aiello, I.; Termine, R.; Golemme, A.; Ghedini, M.; Bellec, N.; Pini, E.; Rimoldi, I.; Godbert, N. Electropolymerized highly photoconductive thin films of cyclopalladated and cycloplatinated complexes. *ACS Appl. Mater. Interfaces* **2015**, *7*, 4019−4028.
(94) Susumu, K.; Therien, M. J. Decoupling Optical and Potentiometric Band Gaps in π-Conjugated Materials. *J. Am. Chem. Soc.* **2002**, *124*, 8550−8552.
(95) Pan, A.; Zhu, X. Optoelectronic properties of semiconductor nanowires. *Semicond. Nanowires* **2015**, 327−363.

https://dx.doi.org/10.1021/acs.inorgchem.0c00491
Inorg. Chem. XXXX, XXX, XXX−XXX